Hindawi
Science and Technology of Nuclear Installations
Volume 2022, Article ID 8098585, 9 pages
https://doi.org/10.1155/2022/8098585

*Research Article*

# High-Temperature Corrosion Behavior of Incoloy 800H Alloy in the Impure Helium Environment

**Wei Zheng, Huang Zhang, Bin Du, Haoxiang Li, Huaqiang Yin, Xuedong He, and Tao Ma**

*Institute of Nuclear and New Energy Technology, Key Laboratory of Advanced Reactor Engineering and Safety of Ministry of Education, Tsinghua University, Beijing, China*

Correspondence should be addressed to Huaqiang Yin; yinhuaqiang@tsinghua.edu.cn

Received 25 July 2022; Revised 3 December 2022; Accepted 6 December 2022; Published 16 December 2022

Academic Editor: Afaque Shams



The helium coolant in the primary circuit of the high-temperature gas-cooled reactor (HTGR) contains traces of impurities, which can induce the corrosion of superalloys when exposed to elevated temperatures. The superalloy damage caused by the corrosion could threaten the safe operation of the reactor. In this work, the corrosion behavior of a representative superalloy (chromium-rich iron base alloy Incoloy 800H) was investigated under the impure helium at different typical temperatures of HTGR. An experimental setup developed for studying the high-temperature corrosion of superalloys was used to investigate the chemical reactions and corrosion behaviors of Incoloy 800H. It was found that $CO_2$ is an important oxygen source in the reaction with chromium, and CO is released as the product. In addition, the observation and computation of the critical temperature ($T_C$) of the reaction between $CO_2$ and carbon in the alloy show that $T_C$ is much lower than that ($T_A$) of the microclimate reaction, which indicates that $CO_2$ can protect the scale from destruction. Furthermore, the slight decarbonization of the alloy was found above $T_C$. Also, a model developed by the thermodynamic analysis was proposed to explain the mechanism of slight decarbonization and predict the critical temperature when the $CO_2$-C reaction occurs. This work presents a guideline for protecting the oxide scale of superalloys used in HTGR.

## 1. Introduction

The high-temperature gas-cooled reactor (HTGR) is a Generation IV nuclear reactor featured with a high outlet coolant temperature that could reach 950°C. Since HTGR has a high operating temperature, it can be used for electricity generation, hydrogen production, and other industrial plants requiring high-temperature process heat. Hence, HTGR is economically competitive in the field of Generation IV nuclear energy technology [1–3]. For cooling HTGR and transferring its heat, helium is considered as the coolant since it is an inert gas that hardly reacts with materials [4]. However, the coolant helium could be polluted by impurities, such as $H_2$, CO, $CH_4$, $H_2O$, and $CO_2$ (these partial pressures are usually in the range of 0.1–100 Pa) [5], from different sources. Graham [6, 7] summarized these sources in HTGR as follows: air from fuel element charge/discharge operations, vapor and carbon oxides from the degassing of the graphite and the thermal insulation or from direct leakage, and hydrogen from proton diffusion through heat exchangers, boilers or reformers. On the other side, the content of impurities is controlled at trace levels by the purification plant. Hence, the helium with these trace impurities is called "HTR-He" [6].

Although the contents of impurities are very low [5], they can interact with structural materials in the steam generator of HTGR at high temperatures. The interaction can gradually deteriorate the performance of structural materials. Therefore, Ni-based and Fe-based alloys, which have good creep performance and high strength as well as the formation of the continuous compact scale on the alloy surface for resisting deep corrosion, are selected as the candidate materials for intermediate heat exchanger (IHX) of the steam generator of HTGR [8, 9]. Hence, the study on the corrosion behavior of Ni-based and Fe-based alloys is significant for the safe operation of the steam generator. The

main corrosion behaviors, including carburization, decarburization, and oxidation, can significantly influence the performance of structural materials [2–13]. Kurata et al. [12, 13] demonstrated that severe carburization may cause a reduction in the creep rupture ductility, and decarburization can lead to a significant loss of creep strength, even though Hastelloy *X* and the variants XR and XR-II (Ni-based alloys) perform good corrosion resistance in the atmosphere of impure helium at 950°C. The oxidation behavior of alloys can be divided into the formation of scale or internal oxide. Rouillard et al. [8] investigated the corrosion behavior of Haynes 230 alloy and proposed that the dense and adherent surface oxide scale can protect the alloy from further rapid corrosion. However, Tsai et al. [10] thought that internal oxidation might cause a reduction in the creep resistance of the alloy due to the tensile stress in the perpendicular direction. In addition, the corrosion behaviors of other superalloys, such as Inconel 617 and Nimonic 86, have been investigated over the past several decades [6, 7].

For most Ni (Fe)-based alloys, a typical corrosion behavior is found that the oxide scale experiences a "destructive reaction" as the temperature increases [8, 9], which results in gradually losing the corrosion resistance of the oxide scale. Brenner and Graham termed this reaction as the "microclimate reaction" [14], which has been observed in experiments [14–16]. This reaction can be written as follows:

$$Cr_2O_3\,(s) + 3C\,(sol) \longrightarrow 3CO\,(g) + 2Cr\,(s). \quad (1)$$

Previous studies [15] have suggested that the operating temperature should be below the reaction temperature ($T_A$) to avoid the loss of the oxide scale. However, this method that controls the operating temperature might reduce the thermal efficiency and economy of HTGR. In order to avoid the loss of oxide scale while keeping a relatively high efficiency, trace $CO_2$ can be introduced as the oxygen source instead of $Cr_2O_3$ in the reaction (1). Meanwhile, $CO_2$ can be used as an oxidant to react with chromium to form an oxide scale on the alloy surface. By controlling $CO_2$ at a proper level in the helium atmosphere, the alloy can be protected against deep corrosion by the continuous oxide layer, while the reactor can be maintained at a high temperature.

The Incoloy 800H has been used as a structural material for the steam generator in the Pebble-bed Modular High-Temperature Gas-cooled Reactor (HTR-PM) in China [17]. To the best of our knowledge, although this alloy was also used and tested in the German HTGR program [7], studies on the gas-phase results of impurities and the corrosion behavior of Incoloy 800H are still limited [18]. Hence, we are interested in studying the typical corrosion behaviors that include the oxidation and carbon transfer of Incoloy 800H at high temperatures.

Particularly, our work is concentrated on investigating the high-temperature corrosion of the Incoloy 800H in impure helium under the temperatures of 500°C, 800°C, and 950°C. The focus is made on the oxidation of $CO_2$ and the slight decarbonization of the alloy above the critical temperature named $T_C$ ("C" stands for "critical"), which is the temperature when $CO_2$ reacts with C and CO is released as the product. Furthermore, the relationship between $T_C$ and partial pressures of CO and $CO_2$ can be obtained by thermodynamic calculation. And the prediction model of the $CO_2$-C reaction is established. Finally, other three corrosion experiments with different CO contents are carried out to verify this model which shows a good agreement with the experimental data.

## 2. Materials and Methods

The schematic and actual pictures of the experimental setup are shown in Figures 1(a) and 1(b), respectively. The setup consists of a configuring system of impure helium and a high-temperature corrosion system. The configuring system can mix various impurities into helium at a wide level from 0 Pa to 100 Pa. This configuring method could cover almost all the atmospheres of impure helium of HTGR, and it is more convenient and cheaper than the purchased standard gases. As shown in Figure 1, pure helium and impurities, such as hydrogen, carbon monoxide, carbon oxide, and methane, are injected into the high-pressure gasholder to be mixed, which is controlled by the mass flow controllers (MFCs). The impure helium prepared is monitored using a gas chromatograph (GC-6600, Fan Wei, China). The main part of the corrosion system is a high-temperature furnace (ZHONG HUAN ELECTRIC FURNACE, China). The holder and furnace tube are made of quartz to avoid device influence on the atmosphere of impure helium at elevated temperatures. In our experiment, a blank test without any samples was carried out to verify that the device did not react with impurities and that no significant gas/gas reactions occurred.

The material used for the corrosion study was a commercial-grade Incoloy 800H plate from WUXI JIAYUN (Jiangsu, China). The chemical composition of Incoloy 800H is shown in Table 1 according to analysis certificates by the manufacturer. Also, no thermal treatment was carried out before the corrosion test. The specimens were cut into 20 mm × 8 mm × 1 mm coupons, polished by the abrasive papers, ultrasonically degreased in ethanol, and dried in air. In each corrosion test, two specimens were placed in separate holders and housed in a high-temperature furnace.

Before the test, the circuits were evacuated to less than $10^{-3}$ Pa and flushed with pure helium until no impurities could be detected. After that, the impure helium was injected into the corrosion system. During the experiment, gas compositions were analyzed both at the inlet and the outlet of the furnace by a gas chromatograph. Table 2 reports the inlet impurity contents in the helium, which is the widely accepted level for a high-temperature corrosion test in HTGR [8–13]. The only difference between this experiment and previous studies is that $CO_2$ was added to the helium. The flow rate of the impure helium was maintained to be 300 mL·min$^{-1}$ [8] by the mass flow controller. Also, the reaction pressure was set to be the atmospheric pressure. The flow rate, about 0.6 mL·s$^{-1}$·cm$^{-2}$, is similar to previous corrosion tests [8, 9, 15, 16]. The samples were heated up at a rate of 2°C·min$^{-1}$ to the preset temperatures of 500°C, 800°C, and 950°C (three separate tests and two samples for each

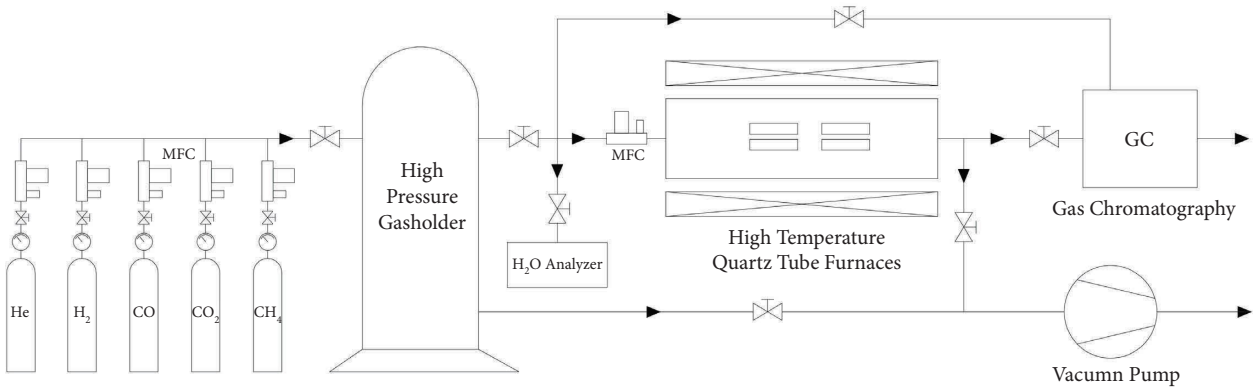


(a)


(b)

Figure 1: (a) The schematic drawing of the system for high-temperature corrosion under impure helium and (b) the actual picture of the experimental facilities: (1) pure gas cylinder, (2) injection equipment for pure gas consisting of multiple mass flow controllers, (3) vacuum pump, (4) high-pressure gasholder, (5) mass flow controllers, (6) high-temperature furnace, (7) gas chromatography, and (8) water analyzer.

Table 1: Composition of the Incoloy 800H alloy before the test (wt.%).

| Alloy | C | Cr | Fe | Ni | Mn | Al | Si | Cu | Ti |
|---|---|---|---|---|---|---|---|---|---|
| Incoloy 800H | 0.084 | 21.28 | Base | 30.96 | 0.97 | 0.249 | 0.320 | 0.120 | 0.251 |

Table 2: Impurity contents in helium at atmospheric pressure (101325 Pa).

| Impurities | $H_2$ | $CH_4$ | CO | $CO_2$ | $H_2O$ |
|---|---|---|---|---|---|
| Partial pressure (Pa) | 55 | 0.25 | 0.58 | 6.4 | 0.10 |

one), and isothermally reacted with the impurities at the fixed temperature for 20 hours. After that, the samples were cooled down at a rate of $3^{\circ}C \cdot min^{-1}$ to room temperature.

The specimens were weighed with high-precision electronic balance (accuracy of 0.1 mg, XPR205, METTLER TOLEDO, Switzerland) before and after the corrosion test. Field emission scanning electron microscopy (FESEM, JEOL JSM-7001F, Japan) with energy-dispersive X-ray spectroscopy (EDS), X-ray diffraction (XRD, D/max-2550, Japan), and carbon sulfur analyzer (CS800, ELTRA, Germany) were used to observe the microstructures and analyze the composition of the specimens.

## 3. Results and Discussion

First, the gas phase of impurities is discussed in Section 3.1, which shows the chemical reaction involved in the corrosion process. Second, the corrosion behaviors of Incoloy 800H are shown in Section 3.2 by the observation of SEM, EDS, and XRD. Third, based on the thermodynamic theory, a corrosion prediction model of the $CO_2$-C reaction is

established in Section 3.3 and verified by the experimental data. Finally, the $CO_2$-C reaction is compared with the microclimate reaction in Section 3.4, indicating that the introduction of $CO_2$ can protect the oxide scale due to the lower critical temperature.

*3.1. Gas-Phase Analysis.* Since the blank test had proved that there were no significant gas/gas reactions, the gas-phase analysis could indicate the occurrence of substance transfer between the atmosphere and alloys. The partial pressures of the main impurities are shown in Figure 2. Since the variation of $H_2$, $CH_4$, and other impurities is very small, the gas-phase data of CO-$CO_2$ would be mainly analyzed here. In addition, the gas phases at 500°C and 800°C are consistent with those at low and medium temperatures in Figure 2. Thus, the gas-phase process of heating up to 950°C is mainly discussed here.

As shown in Figure 2, the variation of $CO_2$ and CO is almost a mirror image, which indicates that they were involved in the same chemical process. The partial pressure of $CO_2$ began to decrease at around 600°C, but the CO increased, illustrating that oxidation of the alloy may occur led by $CO_2$ at this point [19]. It can be written as the following reaction:

$$x\mathrm{M(s)} + y\mathrm{CO_2(g)} \longrightarrow \mathrm{M}_x\mathrm{O}_y\,\mathrm{(s)} + y\mathrm{CO(g)}, \quad (2)$$

with M = Al, Cr, Mn, and Si. Due to the high activity and content of chromium, it is often considered as the representative element which participates in the oxidation reaction. In addition, other mixed oxides could be formed, but chromium oxide is the main component.

The gas-phase analysis in Figure 2 shows that the consumption of $CO_2$ was around 1.2 Pa and the production of CO was up to 1.5 Pa when the temperature reached 950°C. The phenomenon was inconsistent with the oxidation process, where the ratio of $CO_2$ consumption to CO yield is 1 : 1, showing that there may be another reaction of $CO_2$ and CO as expressed by the following reaction:

$$\mathrm{CO_2(g)} + \mathrm{C(sol)} \longrightarrow 2\mathrm{CO(g)}. \quad (3)$$

The C (sol) is the carbon in solution from the alloy, indicating that this reaction leads to the decarburization behavior, which could also cause a potential threat to the alloy if the amount is large. According to the thermodynamic calculation, the Gibbs free energy ($\Delta G$) of reaction (2) is much larger than that of reaction (3), so $CO_2$ should be mainly involved in the oxidation process. It can also be predicted that the amount of decarbonization of the alloy is slight, which can be verified by the measurement of carbon content in the next section. In addition to the oxidation process, the temperature when CO increased may also be the one at which the reaction (3) occurred, which should be verified by the thermodynamic calculation.

As compared to the reactants and products, reaction (3) is similar to the microclimate reaction (1) [20, 21], but the oxygen source is $CO_2$ rather than the oxide scale. If this reaction can occur before the microclimate reaction, then the oxide scale can be protected from damage. Obviously, there should be a thermodynamic equilibrium temperature for both reaction (1) and reaction (3), called $T_A$ and $T_C$, that determine the priority of these reactions. The mechanism and equilibrium temperature of the reaction will be discussed in later sections.

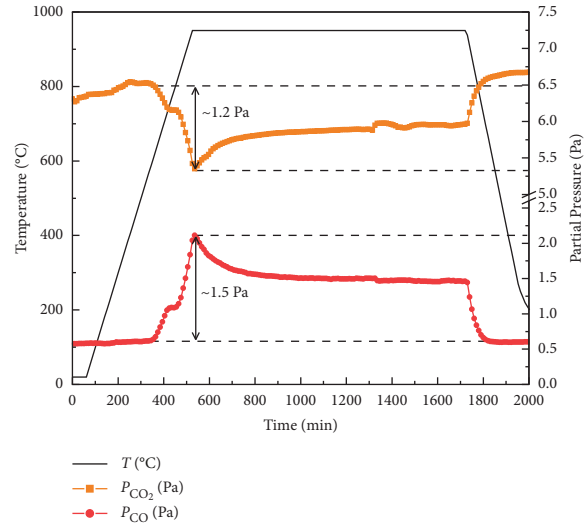


Figure 2: Evolution of the CO and $CO_2$ partial pressure and temperature program as a function of time.

*3.2. Corrosion Behaviors of Alloys.* The samples were weighed before and after the test, and the mass gain per unit of surface area was obtained according to the following equation:

$$\rho_A = \frac{(m_2 - m_1)}{A}, \quad (4)$$

where $\rho_A$ (mg/cm$^2$) is the mass gain per unit surface area, $m_1$ (mg) and $m_2$ (mg) are the weight of samples before and after the test, and $A$ (cm$^2$) is the superficial area. As can be seen from Figure 3, as the temperature increased, the mass gain kept growing, illustrating that there was a significant substance transfer from the atmosphere to the alloy, especially in the high-temperature region. According to the gas-phase analysis (Figure 2), the mass gain is mainly from the oxidation of $CO_2$ in reaction (2), which means that there is no scale reduction and mass loss as in the "microclimate reaction" of Incoloy 800H mentioned by Quadakkers [22]. In addition, Figure 3 also shows the carbon content of alloys at different temperatures, and a slight decrease in carbon content could be observed when the temperature increased above 500°C, which is consistent with reaction (3). As predicted before, the amount of decarbonization is slight, which may be attributed to the blocking effect of the oxide scale.

Figure 4 shows the sample surface of Incoloy 800H exposed at 500°C, 800°C, and 950°C for 20 h, respectively. As the temperature increased, a continuous scale could be gradually observed to form, and the main component was oxide, which can be verified by the oxygen element distribution in EDS results (Figure 5) and the major phase in XRD

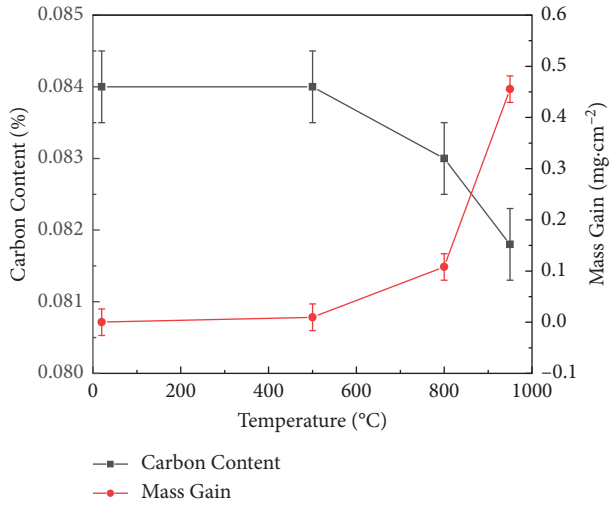


FIGURE 3: Mass gains and carbon content of the alloy 800H after the corrosion test.

results (Figure 6). As shown in Figure 4, when the temperature reached 950°C, the oxide layer was about 3 $\mu$m and the internal oxidation appeared in the range of 10 $\mu$m. This phenomenon indicates that the thinning of the oxide scale led by a "microclimatic reaction" has not occurred, and instead of the oxide scale, $CO_2$ was involved in the carbon transfer reaction. The internal oxide was mainly composed of $Al_2O_3$, which was not continuous and was about 10 $\mu$m deep inside the alloy below the scale. It is consistent with the corrosion behavior of Haynes 230 tested by Rouillard [8], who thought that some Al oxidized along grain boundaries inside the alloy.

Meanwhile, the Cr element distribution in the EDS image is basically similar to that of oxygen, showing that the oxide scale is mainly composed of chromium oxide, which could be verified by XRD (Figure 6). The main phases on the sample surface obtained by XRD analysis are listed in Figure 6, including the Fe-Ni matrix, chromium oxide, iron-manganese oxide, and iron-chromium oxide. At 500°C, there were almost no oxide phases on the surface, only the Fe-Ni elements, which is consistent with the results of SEM and EDS. With the increase in temperature, more oxide phases were generated on the alloy surface. The results of XRD proved that Incoloy 800H under impure helium at 950°C formed a mixed (Fe, Cr, Mn) oxide and $Cr_2O_3$ on the alloy surface, which is similar to the corrosion result of Alloy 230 [9]. Due to the content and activity of the elements, the $Cr_2O_3$ is the main oxide product on the alloy surface in reaction (2).

*3.3. Reaction Mechanism and Model.* According to the measurement results of the carbon content, it can be confirmed that there was slight decarburization of the Incoloy 800H in the impure helium. When the temperature increased, the carbon in the bulk alloy was oxidized by $CO_2$ and it detached from the alloy, leading to the decarbonization phenomenon. It can be described by the following reaction:

$$CO_2\,(g) + C\,(sol) \longrightarrow 2CO\,(g). \tag{5}$$

From the thermodynamic perspective, there is an equilibrium temperature ($T_C$) in reaction (3). When $T > T_C$, the reaction moves to the right side, namely, the decarbonization behavior would occur, so it can be named as "critical temperature." Then, the equilibrium constant can be expressed as follows:

$$K_1\,(T_C) = \frac{P_{CO}^2}{a_C P_{CO_2}}, \tag{6}$$

where $K_1$ is the equilibrium constant of reaction (3), $P_{CO}$ and $P_{CO2}$ are the partial pressure of CO and $CO_2$, and $a_C$ means the carbon activity in the alloy. The equilibrium constant can be obtained by the thermodynamic calculation in Ref. [23, 24] as follows:

$$K_1\,(T_C) = \exp\left[\frac{-\Delta rG}{(R \cdot T_C)}\right], \tag{7}$$

where $\Delta rG$ is the free enthalpy [23] of reaction (3) (kJ/mol) and $R$ is the universal gas constant (J/mol·K). Considering the combination of (6) and (7), the equilibrium temperature can be written as follows:

$$T_C = \frac{-\Delta rG}{\left(R \ln P_{CO}^2 / a_C P_{CO_2}\right)}. \tag{8}$$

Assuming that the carbon and carbides, or more specifically $Cr_3C_2$ or $Cr_{23}C_6$, are in an equilibrium within the substrate [17, 18], then the carbon activity can be obtained by the following reaction:

$$Cr_{23}C6\,(s) \longrightarrow 6C\,(s) + 23Cr\,(s). \tag{9}$$

Therefore, the carbon activity in the alloy is determined by

$$a_C = \frac{K_2\,(T)^{1/6} \cdot a_{C_{r23}C_6}^{1/6}}{a_{C_r}^{23/6}}, \tag{10}$$

where $K_2$ is the equilibrium constant of the reaction (9) and the other three items are the activities of carbon, chromium, and chromium carbide. The method to obtain the equilibrium constant is similar to $K_1$ and the carbide activity ($a_{Cr23C6}$) is taken as the unity [9]. Then, the activity of chromium is the only unknown factor. The accurate data on chromium activity has been a difficult problem for a long time, and the measurement of vapor partial pressure of alloy is a common method to obtain the thermodynamic activity [25]. In this work, the $a_{Cr}$ of Incoloy 800H can be obtained according to Ref. [26].

The theoretical relationship between $T_C$, $P_{CO}$, and $P_{CO2}$ can be obtained by combining equations (8) and (10). Then, when the partial pressures of CO and $CO_2$ are measured, the critical temperature ($T_C$) at which the reaction occurs can be calculated. Therefore, a model can be developed to predict the critical temperature ($T_C$) at which the decarbonization behavior of the alloy occurs in the impure helium containing $CO_2$ and CO.

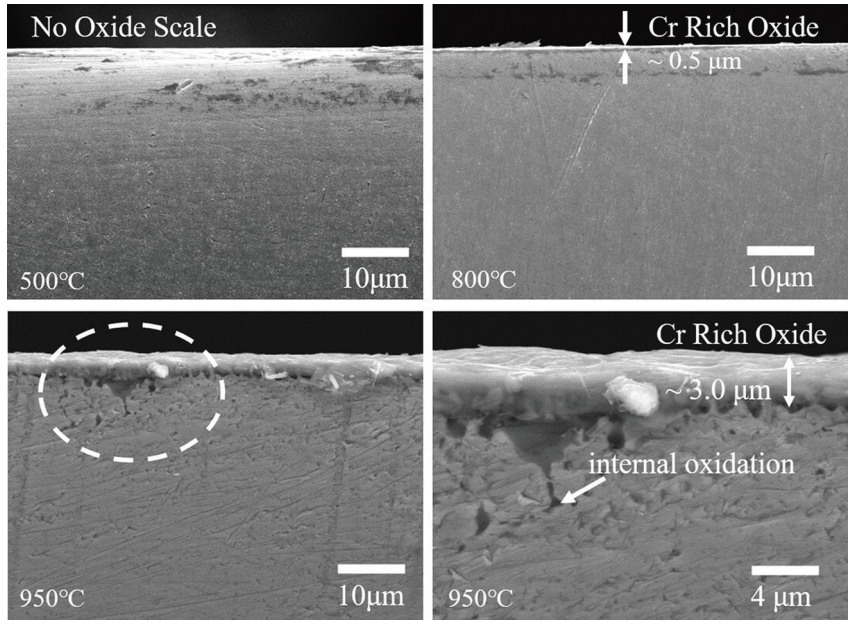


Figure 4: FESEM picture at 20 keV with an SEI (secondary electron imaging) contrast; Incoloy 800H under impure helium at 500°C, 800°C, and 950°C.

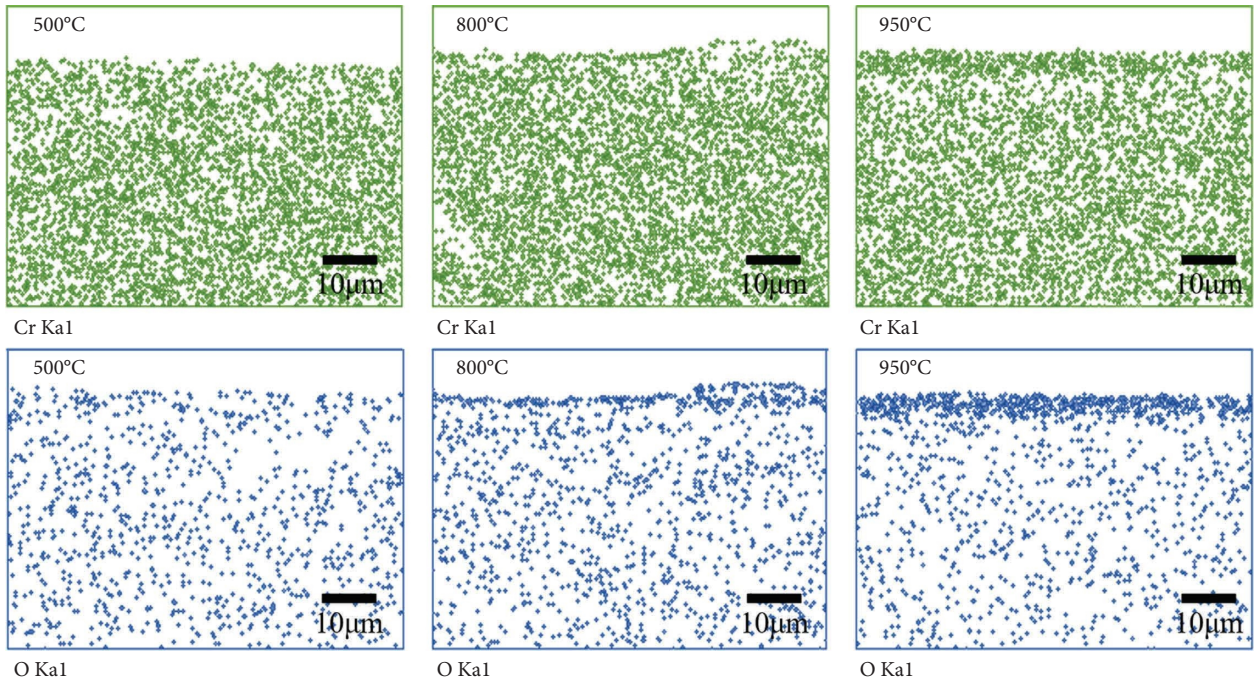


Figure 5: EDS analysis result of oxygen and chromium elements in Incoloy 800H under impure helium at 500°C, 800°C, and 950°C.

According to the thermodynamic analysis, the reaction mechanism and prediction model have been described in detail. Then, it should be verified by gas-phase data in the corrosion test. In this research, when $P_{CO} = 0.58$ Pa and $P_{CO2} = 6.4$ Pa, the temperature at which CO began to increase was about 600°C, as shown in Figure 3. In order to avoid the bias caused by gas-phase fluctuations, the experimental method for measuring $T_C$ is similar to the microclimate reaction [19, 20], namely, it was the temperature for which the increase in the CO partial pressure between the furnace inlet and outlet is equal to 0.1 Pa. Therefore, $T_C$ can be identified as about 620°C in this impure helium, and this value is calculated as 550°C by the prediction model.

However, the release of CO from the reaction between $CO_2$ and Cr may also occur around this temperature, which may lead to the deviation of the $T_C$ measurements. In order to strengthen the accuracy of the prediction model verification, the other three experiments were carried out, in

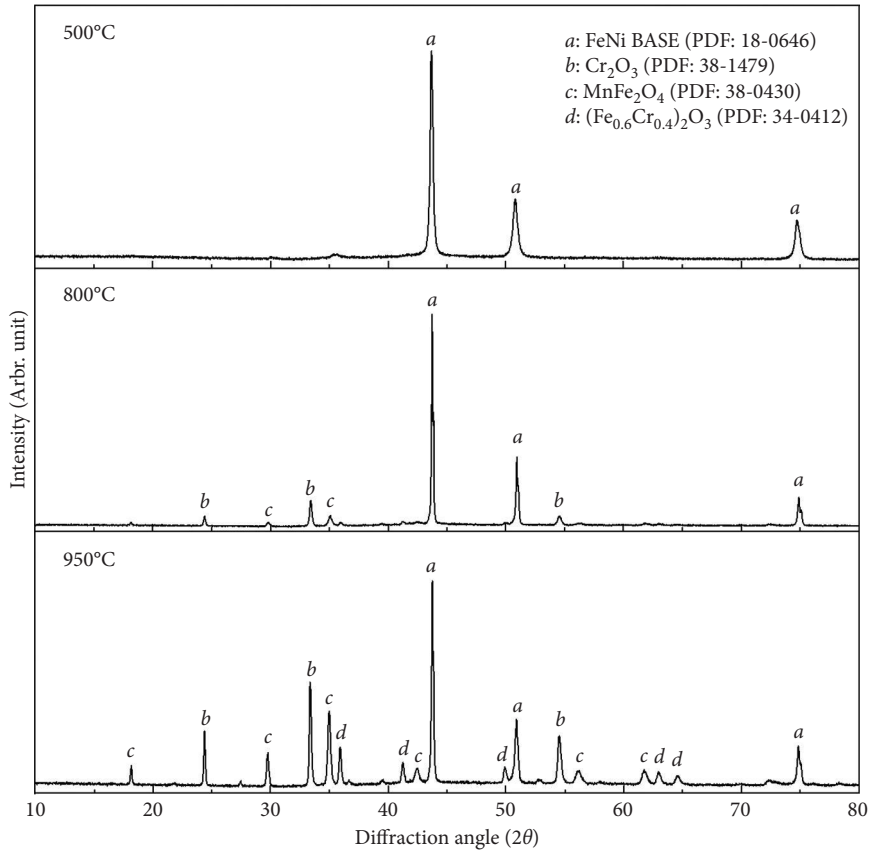


Figure 6: Grazing XRD analysis of Incoloy 800H surface in impure helium at 500°C, 800°C, and 950°C.

which the CO partial pressures were set as 7.0 Pa, 22.5 Pa, and 51.2 Pa and constant $P_{CO2}$. The gas-phase data during the heating process is shown in Figure 7, and the critical temperature $T_C$ can be obtained by the method of "$\Delta P_{CO} = 0.1$ Pa."

As shown in Figure 8, the function curve of alloy 800H obtained through the thermodynamic calculation can express the relationship between CO, $CO_2$, and critical temperature $T_C$. When the $CO_2$ partial pressure is fixed, the higher the CO partial pressure is, the higher the $T_C$ is. The experimental results are in good agreement with the prediction model, and they can be used to predict the temperature at which the carbon transfer behavior occurs in a given impure helium atmosphere containing traces of CO and $CO_2$. However, there are still some errors between the experimental data and the model, especially at low temperatures. It can be attributed to the following two possible reasons: (1) the critical temperatures at the test points are not exactly the equilibrium temperature of the reaction (3), which is an approximated value; (2) the activities of carbon and chrome are not experimental data, and the activity coefficients obtained by fitting may differ from the real values. However, this model still has important guiding significance for the experiment.

*3.4. Comparison with Microclimate Reaction.* Compared with the microclimate reaction (1), the introduction of $CO_2$ can protect the oxide scale from damage, which is mainly related to reactions (2) and (3).

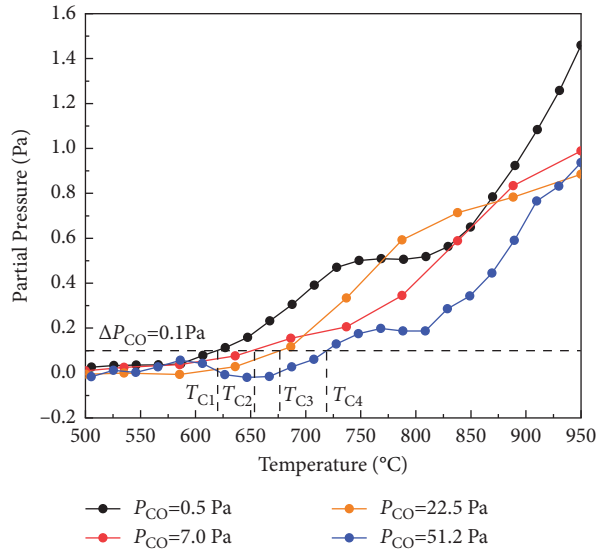


Figure 7: Evolution of the CO as a function of temperature during the heating process.

First, $CO_2$ participated in the oxidation process in reaction (2) and CO was released, leading to an increase in the CO level in the atmosphere. And the equilibrium of reaction (1) is on the left-hand side, so the oxide scale could be inhibited from participating in reaction (1). Secondly, in

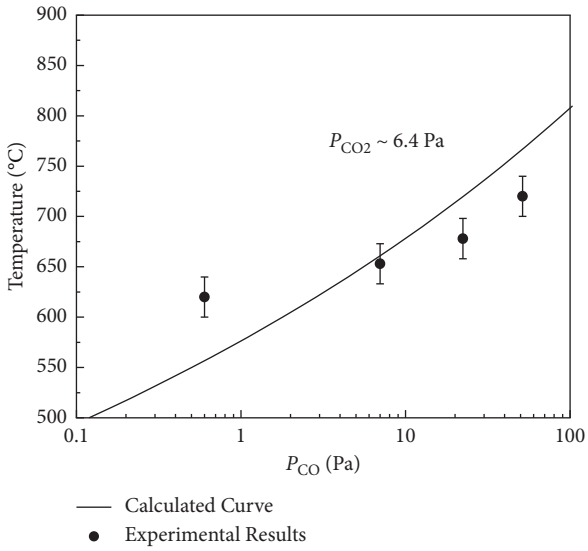


Figure 8: $T_C = f(P_{CO})$ for Incoloy 800H-experimental data and theory.

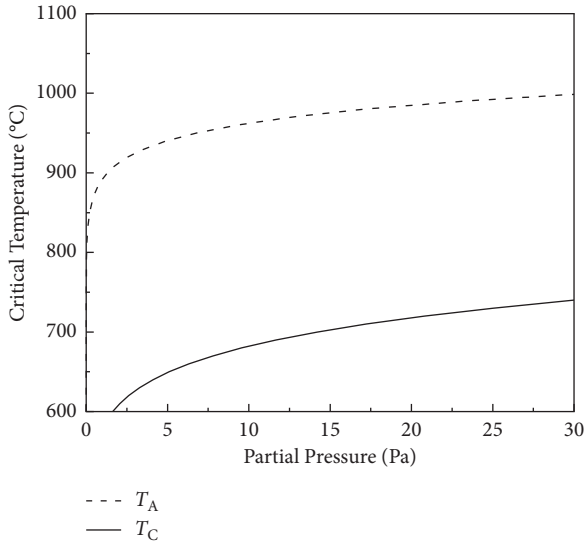


Figure 9: $f(T_C) = P$ (CO) for Incoloy 800H-experimental data and theory.

reaction (3), $CO_2$ directly replaced $Cr_2O_3$ to participate in the microclimate reaction, thereby avoiding the reduction of the oxide layer. However, the premise of the occurrence of reaction (3) is $T_C << T_A$. According to thermodynamic calculations, the critical temperature models for reaction (2) and reaction (3) are given in Figure 9, indicating that $T_C << T_A$ at any CO partial pressure, thus verifying the rationality of $CO_2$ instead of oxides in the reaction.

## 4. Conclusions

The isothermal corrosion tests were carried out for Incoloy 800H, which was used in the steam generator in the HTR-PM, in impure helium at 500°C, 800°C, and 950°C. The corrosion behaviors were analyzed and discussed based on the SEM, EDS, XRD, and carbon sulfur analysis. The reaction mechanism was investigated by thermodynamic analysis and gas-phase data, and a model was developed to rationalize the variation of the critical temperature for carbon transfer $T_C$ as a function of the CO and $CO_2$ partial pressure in the gas phase, which can be used to predict the temperature at which the carbon transfer behavior occurs in a given atmosphere. More specifically, this study presents the following findings:

(1) Incoloy 800H was mainly oxidized by $CO_2$, releasing a large amount of CO. And the oxide scale was mainly composed of mixed (Fe, Cr, and Mn) oxide and $Cr_2O_3$ on the alloy surface

(2) As the temperature rose, the thickness of the oxide layer gradually increased and more oxide phases was observed

(3) The carbon inside the alloy would react with $CO_2$ to produce CO at high temperatures, which would lead to the phenomenon of slight decarbonization of the alloy

(4) $T_C$ is the critical temperature at which the decarbonization would occur. And when the $CO_2$ partial pressure is constant, the higher the CO partial pressure is, the higher the $T_C$ is. Experimental values and the theoretical predictions for $T_C$ are in good agreement

(5) Compared to the "microclimate reaction," it can be found that the oxide layer destruction can be overcome if trace $CO_2$ is introduced as the oxygen source instead of $Cr_2O_3$ in the CO production reaction due to $T_C << T_A$

In general, due to the long-term service of Incoloy 800H in the reactor, it is particularly necessary to investigate the high-temperature corrosion of the alloy. The alloy resistance relies on the growth of a protective surface scale, and the reduction of the scale represents a major risk to the material integrity. Therefore, a method that traces $CO_2$ introduced as the oxygen source in impure helium was proposed to protect the oxide scale from damage. This method can improve the corrosion resistance of alloys, which is very valuable for the long-term operation of HTGR.

## Data Availability

The parameters of the gas phase and microstructure of Incoloy 800H were obtained based on high-temperature corrosion tests, which were used to support the findings of this study and are included within the article.

## Conflicts of Interest

The authors declare that they have no conflicts of interest.

## Acknowledgments

This work was supported by the National Key R&D Program of China (2020YFB1901600), the National Natural Science Foundation of China (No. 11875176), the

Natural Science Foundation of Beijing (Grant no. 3212017), and the National S&T Major Project (Grant no. ZX06901). The research study was supported by the Modular HTGR Supercritical Power Generation Technology collaborative project between CNNC and Tsinghua University (Project no. ZHJTJZYFGWD2020).

## References

[1] Z. Zhang, Z. Wu, D. Wang, and J. Tong, "Development strategy of high temperature gas cooled reactor in China," *Strategic Study of CAE*, vol. 21, no. 1, pp. 12–19, 2019.

[2] S. Fujikawa, H. Hayashi, T. Nakazawa et al., "Achievement of reactor-outlet coolant temperature of 950°C in HTTR," *Journal of Nuclear Science and Technology*, vol. 41, no. 12, pp. 1245–1254, 2004.

[3] C. Jang, D. Kim, D. Kim, I. Sah, W. S. Ryu, and Y. Yoo, "Oxidation behaviors of wrought nickel-based superalloys in various high temperature environments," *Transactions of Nonferrous Metals Society of China*, vol. 21, no. 7, pp. 1524–1531, 2011.

[4] W. Zheng, H. Li, Q. Wang et al., "Oxidation behaviors of the high temperature alloys in the impure helium and argon," in *Proceedings of the 2021 28th International Conference on Nuclear Engineering*, vol. 1, October 2021.

[5] N. Sakaba, H. Ohashi, and T. Takeda, "Hydrogen permeation through heat transfer pipes made of Hastelloy XR during the initial 950°C operation of the HTTR," *Journal of Nuclear Materials*, vol. 353, no. 1-2, pp. 42–51, 2006.

[6] D. M. Graham, "High temperature corrosion in impure helium environments," *High Temperature Technology*, vol. 3, no. 1, pp. 3–14, 1985.

[7] L. W. Graham, "Corrosion of metallic materials in HTR helium environments," *Journal of Nuclear Materials*, vol. 171, no. 1, pp. 76–83, 1990.

[8] F. Rouillard, C. Cabet, K. Wolski et al., "High temperature corrosion of a nickel base alloy by helium impurities," *Journal of Nuclear Materials*, vol. 362, no. 2-3, pp. 248–252, 2007.

[9] C. Cabet, J. Chapovaloff, F. Rouillard et al., "High temperature reactivity of two chromium-containing alloys in impure helium," *Journal of Nuclear Materials*, vol. 375, no. 2, pp. 173–184, 2008.

[10] C. J. Tsai, T. K. Yeh, and M. Y. Wang, "High temperature oxidation behavior of nickel and iron based superalloys in helium containing trace impurities," *Corrosion Science and Technology*, vol. 18, no. 1, pp. 8–15, 2019.

[11] M. Shindo, W. J. Quadakkers, and H. Schuster, "Corrosion behaviour of high temperature alloys in impure helium environments," *Journal of Nuclear Materials*, vol. 140, no. 2, pp. 94–105, 1986.

[12] Y. Kurata, Y. Ogawa, and H. Nakajima, "Effect of decarburizing helium environment on creep behavior of Ni-base heat-resistant alloys for high-temperature gas-cooled reactors," *Tetsu-To-Hagane*, vol. 74, no. 2, pp. 380–387, 1988.

[13] Y. Kurata, Y. Ogawa, and H. Nakajima, "Effect of carburizing helium environment on creep behavior of Ni-base heat-resistant alloys for high-temperature gas-cooled reactors," *Tetsu-To-Hagane*, vol. 74, no. 11, pp. 2185–2192, 1988.

[14] K. G. E. Brenner and L. W. Graham, "The development and application of a unified corrosion model for high-temperature gas-cooled reactor systems," *Nuclear Technology*, vol. 66, no. 2, pp. 404–414, 1984.

[15] F. Rouillard, C. Cabet, K. Wolski, and M. Pijolat, "Oxide-layer formation and stability on a nickel-base alloy in impure helium at high temperature," *Oxidation of Metals*, vol. 68, no. 3-4, pp. 133–148, 2007.

[16] J. Chapovaloff, F. Rouillard, P. Combrade, M. Pijolat, and K. Wolski, "Assessing the kinetics of high temperature oxidation of Inconel 617 in a dedicated HTR impure helium facility coupling thermogravimetry and gas phase chromatography," *Journal of Nuclear Materials*, vol. 441, no. 1-3, pp. 293–300, 2013.

[17] J. Li, S. Yang, and L. Yu, "First time localization practice of steam generator tubes of Incoloy 800H for nuclear power plant," *The hot working processes*, vol. 44, no. 18, pp. 92–94, 2015.

[18] J. Berka, M. Vilemova, and P. Sajdl, "Testing of degradation of alloy 800H in impure helium at 760°C," *Journal of Nuclear Materials*, vol. 464, pp. 221–229, 2015.

[19] X. G. Zheng and D. J. Young, "High-temperature corrosion of $Cr_2O_3$-forming alloys in CO-$CO_2$-$N_2$ atmospheres," *Oxidation of Metals*, vol. 42, no. 3-4, pp. 163–190, 1994.

[20] F. Rouillard, C. Cabet, S. Gossé, K. Wolski, and M. Pijolat, "Thermodynamic modelling of the destruction of the surface $Cr_2O_3$ on Alloy 230 in the impure helium atmosphere of a Gas Cooled Reactor," *Materials Science Forum*, vol. 595-598, pp. 429–438, 2008.

[21] C. Cabet, G. Girardin, F. Rouillard, J. Chapovaloff, K. Wolski, and M. Pijolat, "Comparison of the high temperature surface reactivity in impure helium of two materials for gas cooled reactors," *Materials Science Forum*, vol. 595-598, pp. 439–448, 2008.

[22] W. J. Quadakkers, "Corrosion of high temperature alloys in the primary circuit helium of high temperature gas cooled reactors. Part II: experimental results," *Materials and Corrosion*, vol. 36, no. 8, pp. 335–347, 1985.

[23] L. Shi, *Thermodynamics of Alloys*, p. 530, China Machine Press, Beijing, China, 1992.

[24] J. Chapovaloff, G. Girardin, and D. Kaczorowski, "Parameters governing the reduction of oxide layers on Inconel 617 in impure VHTR He atmosphere," *Materials and Corrosion*, vol. 59, no. 7, pp. 584–590, 2008.

[25] F. N. Mazandarany and R. D. Pehlke, "Thermodynamic properties of solid alloys of chromium with nickel and iron," *Metallurgical Transactions A*, vol. 4, no. 9, pp. 2067–2076, 1973.

[26] S. Gossé, T. Alpettaz, S. Chatain, and G. Christine, "Chromium activity measurements in nickel based alloys for very high temperature reactors: Inconel 617, Haynes 230 and model alloys," *Annals of the Royal College of Surgeons of England*, vol. 91, no. 7, pp. 583–590, 2009.